ORIGINAL ARTICLE

A new automated cycle slip detection and repair method for a single dual-frequency GPS receiver

Zhizhao Liu

Abstract This paper develops a new automated cycle slip detection and repair method that is based on only one single dual-frequency GPS receiver. This method jointly uses the ionospheric total electron contents (TEC) rate (TECR) and Melbourne–Wübbena wide lane (MWWL) linear combination to uniquely determine the cycle slip on both L1 and L2 frequencies. The cycle slips are inferred from the information of ionospheric physical TECR and MWWL ambiguity at the current epoch and that at the previous epoch. The principle of this method is that when there are cycle slips, the MWWL ambiguity will change and the ionospheric TECR will usually be significantly amplified, the part of artificial TECR (caused by cycle slips) being significantly larger than the normal physical TECR. The TECR is calculated based on the dual-frequency carrier phase measurements, and it is highly accurate. We calculate the ionospheric change information (including TECR and TEC acceleration) using the previous epochs (30 epochs in this study) and use the previous data to predict the TECR for the epoch needing cycle slip detection. If the discrepancy is larger than our defined threshold 0.15 TECU/s, cycle slips are regarded to exist at that epoch. The key rational of method is that during a short period (1.0 s in this study) the TECR of physical ionospheric phenomenon will not exceed the threshold. This new algorithm is tested with eight different datasets (including one spaceborne GPS dataset), and the results show that the method can detect and correctly repair almost any cycle slips even under very high level of ionospheric activities (with an average Kp index 7.6 on 31 March 2001). The only exception of a few detected but incorrectly repaired cycle slip is due to a sudden increased

Z. Liu (✉)
Department of Land Surveying and Geo-Informatics,
The Hong Kong Polytechnic University, Hung Hom,
Kowloon, Hong Kong
e-mail: lszzliu@polyu.edu.hk

pseudorange error on a single satellite (PRN7) under very active ionosphere on 31 March 2001. This method requires dual-frequency carrier phase and pseudorange data from only one single GPS receiver. The other requirement is that the GPS data rate ideally is 1 Hz or higher in order to detect small cycle slips. It is suitable for many applications where one single receiver is used, e.g. real-time kinematic rover station and precise point positioning. An important feature of this method is that it performs cycle slip detection and repair on a satellite-by-satellite basis; thus, the cycle slip detection and repair for each satellite are completely independent and not affected by the data of other satellites.

1 Introduction

The use of GPS carrier phase measurements can deliver highly accurate positioning and navigation solutions if the GPS ambiguities are correctly resolved and carrier phase arc is continuously maintained. Using GPS carrier phase measurements for instance, accuracies of 0.1 mm/year have been obtained in crustal velocity measurement (Hill and Blewitt 2006). To achieve this level of accuracy, the ambiguity of carrier phase measurements must be correctly resolved and maintained, and cycle slip must be correctly repaired. The occurrence of cycle slips breaks the continuity of the carrier phase tracking arc, and each cycle of slip can easily bring in a range error of ~20 cm to the L1 measurements. Correct cycle slip detection is critical for correct ambiguity parameterization (Xu 2007). There are basically two options available to treat the cycle slips. One is to detect and repair them,

and the other option is to treat them as unknown ambiguities and estimate them together with other parameters in the GPS data processing. The latter option is apparently less desirable since it makes the data processing more complex. In the case of frequent occurrences of cycle slip, the latter option may fail to estimate the cycle slip. Therefore, the first option is more desirable.

Over the past decade, there are two apparent trends in the GPS or GNSS community. First, the real-time kinematic (RTK) GPS has become more and more popular (Fotopoulos and Cannon 2001; Vollath et al. 2002; Hu et al. 2003; Rizos 2007; Grejner-Brzezinska et al. 2007). It has virtually become a routine GPS surveying technique in many applications. Second, the precise point positioning (PPP) technique for both static and kinematic applications has gained a good momentum of research efforts (Zumberge et al. 1997; Gao and Shen 2002; Ge et al. 2008; Bisnath and Gao 2008; Guyennon et al. 2009). In both RTK and PPP applications, the carrier phase measurements are used as the major observable, and the GPS data are normally recorded at a very high rate (1 Hz or even higher). Under kinematic condition, the GPS data are prone to cycle slips (Roberts et al. 2002; Aoki et al. 2009). In addition to RTK and PPP applications, the use of real-time high rate GPS data has also become a trend in scientific research. The International GNSS Service (IGS) has been working toward generating real-time products since almost one decade ago (Fang et al. 2001; Springer and Hugentobler 2001; Dow et al. 2009). Considering the development and requirements in the GPS/GNSS community, a method that can effectively detect and repair cycle slips for real-time high rate GPS data recorded by a single GPS receiver is desired.

In the past, there are many researches on the cycle slip detection and repair such as Bastos and Landau (1988), Gao and Li (1999), Colombo et al. (1999), Bisnath and Langley (2000), Kim and Langley (2001), and Lee et al. (2003). But these methods are based on double-differenced techniques, and they are not suitable for our purpose of processing single GPS receiver data. Moreover, some methods are based on the integration of the GPS and INS data, e.g. Colombo et al. (1999) and Lee et al. (2003), which significantly constrain their feasibility in many applications due to the cost of INS system as well as the complexity of adding an INS system to GPS. A list of the general cycle slip detection methods such as phase–code comparison, phase–phase ionospheric residual, Doppler integration, and differential phases of time have been summarized in Xu (2007). However these methods have their own limitation. The phase–code comparison method is not effective in repairing small cycle slips (e.g. 1–2 cycles) due to the low accuracy of code measurement. We have tested the Doppler integration method, and like the phase–code comparison, it cannot succeed in small cycle slips. The phase–phase ionospheric residual method, which is essentially the geometry-free linear combination,

has a shortcoming of being insensitive to special cycle slip pairs and unable to check on which frequency the cycle slip happen (Xu 2007). Using the method of differential phases of time requires polynomial fittings interpolate or extrapolate the data at the check epoch (Xu 2007). Our trial test indicates that the polynomial cannot guarantee a success all the time, particularly when the size of cycle slip is small.

Compared to the research based on double-differencing GPS data, the research of cycle slip detection using single GPS receiver data is limited. The work in Blewitt (1990) might be first effort of cycle slip detection and repair for single GPS data. In that paper, an automatic editing algorithm was proposed to simultaneously use the wide-lane combination and ionospheric combination to detect the cycle slip. The wide-lane combination used in Blewitt (1990) is essentially the same as the Melbourne–Wübbena linear combination (Melbourne 1985; Wübbena 1985). This combination is a very effective for cycle slip detection because of its low level of noise and insensitive to ionospheric changes. The ionospheric combination used in Blewitt (1990), which is also called geometry-free combination, however contains the ionospheric residual, and this residual affects the performance of the algorithm. Incorrect cycle slip determination may be caused when there are rapid ionospheric variations (Blewitt 1990). Therefore, a new cycle slip detection method that is more robust under ionospheric variation condition has to be developed. de Lacy et al. (2008) used Bayesian approach to detect cycle slip for single GNSS receivers. This method is based on multiple linear combination and polynomial fitting. The basic assumption of this method is that the original signal is smooth, and discontinuities (i.e. the cycle slip in carrier phase measurements) can be reasonably modeled by a multiple polynomial regression (de Lacy et al. 2008). This assumption may be valid in most cases, but it is very likely violated by the ionospheric disturbance when the GNSS data are observed under high level of ionospheric activities. The test results were based on the GNSS data collected during 23–27 May 2005 (de Lacy et al. 2008). Those days had very low ionospheric activities, and the daily average Kp index varied between 0.0 and 1.2. de Lacy et al. (2008) did not discuss the performance of that method during active ionospheric conditions. More recently, a method using triple GPS frequencies to detect cycle slip has been proposed (Dai et al. 2008, 2009). This method in theory can be applied to dual-frequency GPS signals although it is designed for three frequency GPS signals. This method relies on the proper selection of the scale (ω_i) for each combined observation (the total number of observations is n) to meet the requirement $\sum_{i=1}^{n} \omega_i = 0$ and to produce the minimum standard deviation of the combined observation. In this method, the ionospheric residual is ignored (Dai et al. 2008, 2009). This might be an issue when the ionosphere undergoes rapid variations. It was stated that in some situations for instance magnetic storm, the detection

approach may provide unexpected results (Dai et al. 2009). As a matter of fact, at present there is only one modernized GPS satellite in space broadcasting signals at L1, L2, and L5 three frequencies. The use of dual-frequency GPS receivers and satellites is still prevailing in the applications.

In this paper, a new cycle slip detection and repair method that employs the ionospheric total electron content (TEC) rate (TECR) is proposed. Unlike other methods where the ionospheric variation is regarded as a nuisance or simply ignored, in this method, the ionospheric variation, characterized by the TEC rate, is precisely estimated and used to detect and repair cycle slip. Without cycle slips, the ionospheric physical TECR is normally bounded by a certain value. In this study, we choose the threshold value as 0.15 TECU/s. When there are cycle slips, the ionospheric TECR will become significantly larger, with most contribution from the artificial ionospheric TECR that is resulted from cycle slips. The Melbourne–Wübbena wide lane (MWWL) ambiguity will also change when there are cycle slips. With the data of both ionospheric TECR change and MWWL ambiguity change, the cycle slips can be precisely and uniquely determined.

This paper is organized as below. The methodology of detecting and repairing cycle slip is developed in detail in Sect. 2. The accuracies of the estimated cycle slip terms are analyzed too. The analyses of the method performance are performed in Sect. 3. In Sect. 4, the application of this method is discussed. The conclusion is given in Sect. 5.

2 Methodology

In this cycle slip detection and repair method, two sets of measurements are jointly employed to precisely determine the size of the cycle slips. One is the Melbourne–Wübbena linear combination that has been widely used for cycle slip detection and ambiguity resolution because of its 86-cm long wavelength (Melbourne 1985; Wübbena 1985; Blewitt 1990; Kass et al. 2009; Bock et al. 2009). This combination removes the effects from the atmosphere (including both ionosphere and troposphere), the geometry, and the satellite and receiver clocks. Therefore, this combination is useful to check GPS observations for cycle slips (Dach et al. 2006). The other set of measurements is the ionospheric TECR that is inferred from L1 and L2 carrier phase measurements.

2.1 Carrier phase and pseudorange observations

We assume that the dual-frequency GPS receiver observes the satellite p. The observation equations for dual-frequency GPS carrier phase and pseudorange measurements can be written as:

$$\lambda_1 \Phi_1^p = \rho^p + c(dt - dT^p) - I + T + \lambda_1 N_1^p, \tag{1}$$

$$\lambda_2 \Phi_2^p = \rho^p + c(dt - dT^p) - \gamma I + T + \lambda_2 N_2^p, \tag{2}$$

$$P_1^p = \rho^p + c(dt - dT^p) + I + T, \tag{3}$$

$$P_2^p = \rho^p + c(dt - dT^p) + \gamma I + T, \tag{4}$$

where λ_1 and λ_2 are the wavelengths of the GPS L1 and L2 signals, respectively; Φ_1^p and Φ_2^p are carrier phase measurements on L1 and L2 frequencies, respectively; P_1^p and P_2^p are the pseudorange measurements; ρ^p is the geometrical distance between the receiver and the satellite p; dt and dT^p are the GPS receiver and satellite clock errors, respectively; c is the speed of light in vacuum; I is the ionospheric range delay on GPS L1 signal; T is the tropospheric range delay; N_1^p and N_2^p are the integer number of cycles for GPS L1 and L2 signals, respectively, which are often called ambiguities; $\gamma = f_1^2/f_2^2$ is the ratio of the squared frequencies of GPS L1 and L2 signals. The carrier phase measurements Φ_1^p and Φ_2^p and the ambiguities N_1^p and N_2^p are in the unit of cycle. The dt and dT^p are in the unit of second. The rest variables are all in the unit of meter.

2.2 Cycle slip determined from the Melbourne–Wübbena wide-lane combination

The well-known MWWL linear combination at a given epoch can be formed as below (Melbourne 1985; Wübbena 1985). The tag for epoch is omitted for brevity.

$$\begin{aligned} L_{MWWL} &= \frac{f_1 \cdot \lambda_1 \Phi_1^p - f_2 \cdot \lambda_2 \Phi_2^p}{f_1 - f_2} - \frac{f_1 \cdot P_1^p + f_2 \cdot P_2^p}{(f_1 + f_2)} \\ &= \lambda_{WL} N_{WL}^p, \end{aligned} \tag{5}$$

where $\lambda_{WL} = c/(f_1 - f_2) \approx 86$ cm and $N_{WL}^p = N_1^p - N_2^p$. The λ_{WL} and N_{WL}^p are called wide-lane wavelength and wide-lane ambiguity, respectively. Thus, the wide-lane ambiguity at a given epoch can be estimated as:

$$N_{WL}^p = \frac{L_{MWWL}}{\lambda_{WL}} = \left[\Phi_1^p - \Phi_2^p - \frac{f_1 \cdot P_1^p + f_2 \cdot P_2^p}{\lambda_{WL}(f_1 + f_2)} \right]. \tag{6}$$

We assume that at epoch $(k-1)$ there are no cycle slips, or the cycle slips have been repaired if any. But at epoch (k) there are cycle slips on both L1 and L2 carrier phase measurements $\Phi_1^p(k)$ and $\Phi_2^p(k)$. The cycle slips are denoted as $\Delta N_1^p(k)$ and $\Delta N_2^p(k)$, respectively. After cycle slips are detected and repaired, the correct carrier phase measurements at epoch (k) should be calculated as:

$$\widehat{\Phi_1^p}(k) = \Phi_1^p(k) + \Delta N_1^p(k), \tag{7}$$

$$\widehat{\Phi_2^p}(k) = \Phi_2^p(k) + \Delta N_2^p(k), \tag{8}$$

where $\widehat{\Phi_1^p}$ and $\widehat{\Phi_2^p}$ denote the correct L1 and L2 phase measurements, respectively, after cycle slips are repaired.

Integrating Eqs. (5)–(8), the cycle slip term $\left[\Delta N_1^{\mathrm{p}}(k) - \Delta N_2^{\mathrm{p}}(k)\right]$ can be estimated as:

$$\left[\Delta N_1^{\mathrm{p}}(k) - \Delta N_2^{\mathrm{p}}(k)\right] = N_{\mathrm{WL}}^{\mathrm{p}}(k-1) - N_{\mathrm{WL}}^{\mathrm{p}}(k). \tag{9}$$

2.3 Accuracy analysis of the cycle slip term $\left[\Delta N_1^{\mathrm{p}}(k) - \Delta N_2^{\mathrm{p}}(k)\right]$

It is known that the GPS carrier phase measurements Φ_1^{p} and Φ_2^{p} are very precise, and the carrier phase can be measured with an accuracy of 1.0 mm or even higher. Even if the multipath and atmospheric effects are considered, the accuracy of the carrier phase measurements is still as good as a few millimeters. Thus, the accuracy of the determined cycle slips $\left[\Delta N_1^{\mathrm{p}}(k) - \Delta N_2^{\mathrm{p}}(k)\right]$ is largely dependent on the error of the pseudorange measurements. Assuming that the code measurements have the equal noise level of σ_{P} (in unit of meter), the standard deviation of term $\frac{f_1 \cdot P_1^{\mathrm{p}}(k-1) + f_2 \cdot P_2^{\mathrm{p}}(k-1)}{\lambda_{\mathrm{WL}}(f_1 + f_2)}$ is equivalent to $\frac{\sqrt{f_1^2 + f_2^2}}{\lambda_{\mathrm{WL}}(f_1 + f_2)} \sigma_{\mathrm{P}}$ cycles, i.e. $0.8267\sigma_{\mathrm{P}}$ cycle. Please note the coefficient $\frac{\sqrt{f_1^2 + f_2^2}}{\lambda_{\mathrm{WL}}(f_1 + f_2)}$ has the unit of cycle/meter. Thus, the standard deviation of $\left[\Delta N_1^{\mathrm{p}}(k) - \Delta N_2^{\mathrm{p}}(k)\right]$, in unit of cycles, is $1.1691\sigma_{\mathrm{P}}$. With today's GPS receiver technology, the pseudorange code observations have a typical accuracy of 0.5 m at $15°$ elevation angle (Sükeová et al. 2007). This indicates that the standard deviation of $\left[\Delta N_1^{\mathrm{p}}(k) - \Delta N_2^{\mathrm{p}}(k)\right]$ estimated by Eq. (9) is approximately 0.5846 cycle. That is to say, the wide-lane ambiguity error, primarily resulting from the pseudorange noise, will normally be less than 0.6 cycle. It was shown that with higher elevation angle, the noise of the pseudorange measurements will decrease (Sükeová et al. 2007). Consequently, the uncertainty contribution from the pseudorange measurements to the cycle slip detection will become smaller. It should be noted that the MWWL is very effective in detecting slips as small as one cycle, but it has its own limitation too. First, the MWWL combination will not signify the occurrence of cycle slips when the cycle slips on L1 and L2 have the same size and same sign since they cancel each other as Eq. (6) shows. Second, when cycle slips are detected, it is impossible to tell if L1 or L2 or both frequencies have the cycle slips. That is why we proposed the ionospheric TECR-based cycle slip detection approach to supplementing the MWWL detection method. It will be shown that the joint use of both methods can effectively detect and distinguish cycle slips under any situations.

2.4 Cycle slip determined from the TECR

From Eqs. (1) and (2), we can derive the ionospheric total electron contents from dual-frequency carrier phase measurements as below (Liu and Gao 2004). It is assumed that we use the GPS data from epoch $(k-1)$.

$$\mathrm{TEC}_\Phi(k-1)$$
$$= \frac{f_1^2 \left\{\left[\lambda_1 \Phi_1^{\mathrm{p}}(k-1) - \lambda_2 \Phi_2^{\mathrm{p}}(k-1)\right] - [\lambda_1 N_1 - \lambda_2 N_2] - b_i - b^{\mathrm{p}}\right\}}{40.3 \times 10^{16}(\gamma - 1)},$$
$$\tag{10}$$

where b_i and b^{p}, in unit of meters, are the inter-frequency biases of the receiver and the satellite, respectively. Other terms in Eq. (10) are the same as those defined in previous equations. The values of satellite and receiver inter-frequency biases are quite stable during a period of a few days (Schaer 1999). Therefore, they can be treated as constants during the cycle slip detection where the time interval between two consecutive epochs is normally as short as 1 s or at most a few minutes.

Similar to the MWWL combination, two consecutive epochs are needed to perform cycle slip detection and repair. We only consider the cycle slip occurrence at epoch (k). The GPS L1 and L2 carrier phase measurements at epoch $(k-1)$ are regarded as free of cycle slips or the cycle slips have already been repaired if they indeed occur at that epoch. If the total electron contents $\mathrm{TEC}_\Phi(k)$ estimated from epoch (k) is differentiated with that of epoch $(k-1)$, the total electron contents rate (TECR) can be derived.

$$\mathrm{TECR}_\Phi(k) = \frac{\mathrm{TEC}_\Phi(k) - \mathrm{TEC}_\Phi(k-1)}{\Delta t}, \tag{11}$$

where $\mathrm{TECR}_\Phi(k)$ is the TEC rate at epoch (k); Δt is the time interval between epochs (k) and $(k-1)$, which is typically 1 s for high rate GPS observations. Rearranging Eqs. (11) and (12), the cycle slips at epoch (k) can be estimated as:

$$\left[\lambda_1 \Delta N_1^{\mathrm{p}}(k) - \lambda_2 \Delta N_2^{\mathrm{p}}(k)\right]$$
$$= \frac{40.3 \times 10^{16}(\gamma - 1)\Delta t \cdot \mathrm{TECR}_\Phi(k)}{f_1^2}$$
$$- \lambda_1 \left[\Phi_1^{\mathrm{p}}(k) - \Phi_1^{\mathrm{p}}(k-1)\right]$$
$$+ \lambda_2 \left[\Phi_2^{\mathrm{p}}(k) - \Phi_2^{\mathrm{p}}(k-1)\right]. \tag{12}$$

It is clear that all the terms in the above Eq. (13) are known except the TEC rate $\mathrm{TECR}_\Phi(k)$. If the $\mathrm{TECR}_\Phi(k)$ is also known, we can then estimate the cycle slip $\left[\lambda_1 \Delta N_1^{\mathrm{p}}(k) - \lambda_2 \Delta N_2^{\mathrm{p}}(k)\right]$. How the $\mathrm{TECR}_\Phi(k)$ is obtained will be discussed in the following section. It should be noted that in Eq. (12) only carrier phase measurements are used; thus, it is expected that the accuracy of the estimated $\left[\lambda_1 \Delta N_1^{\mathrm{p}}(k) - \lambda_2 \Delta N_2^{\mathrm{p}}(k)\right]$ will be very high. This will also be analyzed in the following section.

2.5 The estimation of $\text{TECR}_\Phi(k)$

As illustrated in Eq. (11), the $\text{TECR}_\Phi(k)$ is estimated from the measurements at epoch (k) and its previous epoch $(k-1)$. But we cannot use the Eq. (11) because we are intending to detect cycle slips at epoch (k) and we are not sure if epoch (k) has cycle slips. The $\text{TECR}_\Phi(k)$ however can be estimated based on the measurements of the previous epochs. Since we are detecting and repairing cycle slips on an epoch-by-epoch basis, all the epochs prior to the current epoch (k) are free of cycle slips because their cycle slips, if any, have been repaired. Therefore at epoch (k), we can use the previous epochs to estimate the TEC rate for epoch (k). For instance, at epoch $(k-1)$, we can use the measurements of epochs $(k-1)$ and $(k-2)$ to derive $\text{TECR}_\Phi(k-1)$. At epoch $(k-1)$, if the rate of the TEC rate (i.e. TEC acceleration) is also known, the $\text{TECR}_\Phi(k)$ at epoch (k) can be readily estimated as:

$$\text{TECR}_\Phi(k) = \text{TECR}_\Phi(k-1) + \dot{\text{TECR}}_\Phi(k-1) \cdot \Delta t, \quad (13)$$

where $\dot{\text{TECR}}_\Phi(k-1)$ is the TEC acceleration at epoch $(k-1)$. The determination of the $\dot{\text{TECR}}_\Phi(k-1)$ can be performed as below:

$$\dot{\text{TECR}}_\Phi(k-1) = \frac{\text{TECR}_\Phi(k-1) - \text{TECR}_\Phi(k-2)}{\Delta t}. \quad (14)$$

In the practical implementation, both $\text{TECR}_\Phi(k-1)$ and $\text{TECR}_\Phi(k-2)$ are estimated using measurements of previous epochs. They are averaged to smooth the noise in the measurements (Blewitt 1990). Thus, more accurate $\text{TECR}_\Phi(k-1)$ and $\text{TECR}_\Phi(k-2)$ can be obtained. In our study, 30 previous epochs are used.

2.6 Accuracy analysis of the cycle slip term $\left[\lambda_1 \Delta N_1^p(k) - \lambda_2 \Delta N_2^p(k)\right]$

We assume that all the carrier phase measurements have the equal accuracy, and their standard deviations are denoted as σ_Φ. The uncertainty of $\text{TECR}_\Phi(k)$ is represented by $\sigma_{\text{TECR}_\Phi(k)}$. Thus, the uncertainty of the cycle slip term $\left[\lambda_1 \Delta N_1^p(k) - \lambda_2 \Delta N_2^p(k)\right]$ can be estimated as below while assuming that all the carrier phase measurements are not correlated with each other.

$$\sigma^2_{\left[\lambda_1 \Delta N_1^p(k) - \lambda_2 \Delta N_2^p(k)\right]} = \left(\frac{40.3 \times 10^{16}(\gamma-1)\Delta t}{f_1^2}\right)^2 \sigma^2_{\text{TECR}_\Phi(k)} + 2\left(\lambda_1^2 + \lambda_2^2\right)\sigma^2_\Phi. \quad (15)$$

Considering Eqs. (13) and (14), the variance $\sigma^2_{\text{TECR}_\Phi(k)}$ can be approximately estimated as $5\sigma^2_{\text{TECR}_\Phi(k-1)}$ when the measurements of epochs $(k-1)$ and $(k-2)$ are regarded as uncorrelated and having same accuracies. The $\sigma^2_{\text{TECR}_\Phi(k-1)}$

can be further estimated as below based on the Eqs. (10) and (11).

$$\sigma^2_{\text{TECR}_\Phi(k-1)}$$
$$= \frac{2}{\Delta t^2}\left(\frac{f_1^2}{40.3 \times 10^{16}(\gamma-1)}\right)^2\left(\lambda_1^2 + \lambda_2^2\right)\sigma^2_\Phi. \quad (16)$$

Combining Eqs. (15) and (16), the variance of $\left[\lambda_1 \Delta N_1^p(k) - \lambda_2 \Delta N_2^p(k)\right]$ thus can be estimated as:

$$\sigma^2_{\left[\lambda_1 \Delta N_1^p(k) - \lambda_2 \Delta N_2^p(k)\right]} = 12\left(\lambda_1^2 + \lambda_2^2\right)\sigma^2_\Phi. \quad (17)$$

In Eq. (17), the wavelengths λ_1 and λ_2 are in unit of meter/cycle, and the standard deviation σ_Φ is in the unit of cycle. The variance $\sigma^2_{\left[\lambda_1 \Delta N_1^p(k) - \lambda_2 \Delta N_2^p(k)\right]}$ has a unit of m^2. In practical application, the standard deviation σ_Φ is usually expressed with length unit, e.g. mm after being implicitly multiplied by its wavelength. The carrier phase measurement error inside the receiver is normally small, at about 1 mm level. Considering the noises resulting from multipath and atmospheric effects, the overall carrier phase measurements may have a few millimeters. If we take $\sigma_\Phi = 5$ mm, the standard deviation of the cycle slip term $\left[\lambda_1 \Delta N_1^p(k) - \lambda_2 \Delta N_2^p(k)\right]$ is estimated to be 5.4 mm. It clearly shows that the cycle slip term $\left[\lambda_1 \Delta N_1^p(k) - \lambda_2 \Delta N_2^p(k)\right]$ estimated from the TEC rate data has a very high accuracy. This is due to the sole use of high accuracy carrier phase measurements and no pseudorange measurements being used.

2.7 Cycle slip detection using the MWWL ambiguity

The MWWL cycle slip term, Eq. (9), is estimated independently at each epoch (k). The analysis shows that the uncertainty resulting from the pseudorange measurements is approximately 0.6 cycle. If the cycle slip term $\left[\Delta N_1^p(k) - \Delta N_2^p(k)\right]$ is larger than 1.0 cycle, the epoch (k) is considered having cycle slip with respect to its previous epoch $(k-1)$. This detection is simple and merely depends on two epochs. To be more statistically meaningful, it is suggested that the cycle slip detections should make use of the statistic information of the previous epochs.

The mean and variance of the wide-lane ambiguity can be estimated based on all the data prior to epoch (k). If the cycle slip term $\left[\Delta N_1^p(k) - \Delta N_2^p(k)\right]$ calculated in Eq. (9) is within 4.0 times of the standard deviation, this epoch (k) is most likely to be free of cycle slip (Blewitt 1990). However, it has to be further confirmed by checking the ionospheric TECR to exclude the case $\left[\Delta N_1^p(k) = \Delta N_2^p(k)\right]$, as to be discussed in the below section. If it is larger than the 4.0 times of standard deviation, it is regarded that there are cycle slips. In this case, the cycle slips have

to be determined in conjunction with the TECR information.

The mean and the variance of the MWWL ambiguity at epoch (k) can be recursively calculated as below:

$$E\left[N_{WL}^{p}(k)\right] = \overline{N_{WL}^{p}(k)} = \overline{N_{WL}^{p}(k-1)}$$

$$+ \frac{1}{k}\left[N_{WL}^{p}(k) - \overline{N_{WL}^{p}(k-1)}\right], \quad (18)$$

where $N_{WL}^{p}(k)$ is the wide-lane ambiguity determined by Eq. (6), and $\overline{N_{WL}^{p}(k)}$ is the mean value of $N_{WL}^{p}(k)$. The variance of $N_{WL}^{p}(k)$ can be calculated as below:

$$\sigma^2_{N_{WL}^{p}(k)} = E\left[\left(N_{WL}^{p}(k)\right)^2\right] - \left(\overline{N_{WL}^{p}(k)}\right)^2. \quad (19)$$

The $E\left[\left(N_{WL}^{p}(k)\right)^2\right]$ in Eq. (19) is the mean squared value of $N_{WL}^{p}(k)$, and it is can be recursively calculated as:

$$E\left[\left(N_{WL}^{p}(k)\right)^2\right] = E\left[\left(N_{WL}^{p}(k-1)\right)^2\right]$$

$$+ \frac{1}{k}\left\{\left(N_{WL}^{p}(k)\right)^2 - E\left[\left(N_{WL}^{p}(k-1)\right)^2\right]\right\}. \quad (20)$$

The calculation of the mean value in Eq. (18) is the same as the method in Blewitt (1990). However the calculation of variance is slightly different. In the paper by Blewitt (1990), an initial value of 0.5 cycle was given to the standard deviation at the first epoch and the standard deviation recursive formula is an approximation although it is very close to the true value. Equations (19) and (20) are closed-form expressions. Moreover, calculating Eqs. (19) and (20) does not require an initial value to be given at the first epoch.

2.8 Cycle slip detection using the TECR

To detect the cycle slip at epoch (k), the mean and variance of the TECR data prior to epoch (k) are recursively calculated using the similar approach shown in Eqs. (18)–(20). In this study, we consider the TECR data basically constant over a short period (normally no more than half minute). To be mathematically more rigorous, the filtering approach given in Kee et al. (1997) can be used to estimate the TECR considering the variance differences between epochs. But our extensive test results showed that it is normally adequate to regard the TECR data as a constant in a short period. The TEC acceleration is also calculated to account for the different ionospheric rates between epochs. The TECR calculated at epoch (k), shown in Eq. (11), is compared with the one estimated as $\left[\text{TECR}_{\Phi}(k-1) + \dot{\text{TECR}}_{\Phi}(k-1) \cdot \Delta t\right]$. If their difference, called TECR residual, is within four times of the standard deviation, no cycle slips are assumed at epoch (k). Otherwise, cycle slips are detected, and Eq. (12) is used to determine

the size of the cycle slip term $\left[\lambda_1 \Delta N_1^{p}(k) - \lambda_2 \Delta N_2^{p}(k)\right]$. The TECR residual is composed of the natural ionospheric TECR and the artificial ionospheric TECR. The natural ionospheric TECR results from the natural ionospheric variation at epoch (k), causing the difference between the predicted TECR and actual TECR at epoch (k). The artificial ionospheric TECR is due to the cycle slips of the carrier phase measurements at epoch (k). When there is no cycle slip, the artificial TECR is 0. Otherwise, the artificial TECR is normally nonzero except that the L1 and L2 carrier phases have the special cycle slip pair $(77N, 60N)$, $N = 0, \pm 1, \pm 2, \ldots$. Table 1 lists the artificial TECR caused by some typical cycle slip examples. The first part of Table 1 shows the cycle slips that cause the smallest artificial TECR, and the second part shows the cycle slips that cause the smallest MWWL ambiguity changes. It shows that when the cycle slip pairs are $(77N, 60N)$, $N = 0, \pm 1, \pm 2, \ldots$, the artificial TECR is the smallest (i.e. 0.0 TECU/s). In this special case, we see the cycle slip difference is as large as 17 cycles. Thus, we can still rely on the MWWL ambiguity information to determine the cycle slips. The last six rows of Table 1 show that although the size of cycle slip is small, the resultant artificial TECR is however very large. The leads to the easy cycle slip detection by using the large artificial TECR change.

As said in the above section, even if there is no detectible cycle slip using MWWL linear combination, it cannot exclude the likelihood of $\Delta N_1^{p}(k) = \Delta N_2^{p}(k)$ although it is extremely unlikely (Blewitt 1990). When $\Delta N_1^{p}(k) = \Delta N_2^{p}(k)$ occurs, their impact on the wide-lane ambiguity is null, but they have an effect on the ionospheric TEC rate. The following Table 2 shows a few examples of the effect of the cycle slips on the TEC and TEC rate. It can be seen in Table 2 that even if the cycle slip is only one cycle, its contribution to the TEC is significant, as large as -0.5133 TECU. The TEC change caused by cycle slips is linearly proportional to the size of the cycle slip. The TECR changes caused by cycle slips depend on not only the size of cycle slip but also the data interval. As Table 2 shows when size of slip is one cycle and the data interval is 1.0 s, the cycle slip caused TECR is as large as -0.514 TECU/s. This is approximately 50 times of the nominal TECR value in quiet ionosphere period and 17 times of that in active ionospheric period. It has been shown that in the equatorial region like Hong Kong, the ionospheric slant TEC rate is about 0.01 TECU/s during quiet ionosphere periods, and it rises to 0.03 TECU/s during disturbed ionosphere period (Liu and Chen 2009). Therefore, such a large deviation from the nominal TECR value makes it very easy to detect the cycle slip even if its size is only one cycle.

Table 2 shows that the same size of cycle slip has more prominent impact on the TECR when the data interval is smaller. For instance, when one cycle of slip occurs on data

Table 1 Examples of the smallest artificial TECR and the smallest cycle slips

Cycle slip on L1 (cycle)	Cycle slip on L2 (cycle)	Cycle slip difference (cycle)	Artificial TECR (TECU/s) ($\Delta t = 1.0$ s)
−77	−60	−17	0.000
77	60	17	0.000
−9	−7	−2	−0.030
9	7	2	0.030
−68	−53	−15	0.030
68	53	15	−0.030
−18	−14	−4	−0.060
18	14	4	0.060
−59	−46	−13	0.060
59	46	13	−0.060
–	–	–	–
−1	−1	0	0.514
1	1	0	−0.514
−1	0	−1	−1.812
1	0	1	1.812
0	−1	1	2.326
0	1	−1	−2.326

Table 2 The effect of cycle slip on TEC and TEC rate

$\Delta N_1^p(k) = \Delta N_2^p(k)$ (cycle)	Effect on TEC (TECU)	Effect on TEC rate (TECU/s)	
		Data interval ($\Delta t = 1.0$ s)	Data interval ($\Delta t = 30.0$ s)
1	−0.514	−0.514	−0.017
2	−1.026	−1.026	−0.034
3	−1.540	−1.540	−0.051
4	−2.053	−2.053	−0.068
5	−2.566	−2.566	−0.086

with an interval of 30.0 s, the caused TECR change is only −0.017 TECU/s. This magnitude is very close to the nominal TECR value in quiet ionosphere period and is even smaller than the value under active ionosphere conditions. Thus, it will be a challenge to detect small cycle slip with a low data rate.

It can be seen from Table 2 that the larger size the cycle slip, the larger change to the ionospheric TECR. This in turn makes the cycle slip detection easier. In order to test the effectiveness of this method, we need only to test the case with the smallest cycle slip, i.e. $\Delta N_1^P(k) = N_2^P(k) = -1$ cycle using the GPS data. In addition to the cycle slip pair $(-1, -1)$ on L1 and L2 frequencies, we will also test two other cycle slip pairs: $(-9, -7)$ and $(-77, -60)$. The reason for choosing these cycle slip pairs is elaborated in the following section.

3 Data test and analysis

3.1 Data description

The effectiveness of this method was extensively tested using eight sets of 24-h GPS observations (except the seventh set containing only approximately 4.5 h data) that were collected with different receiver dynamics, at different locations, in different days and under different levels of ionospheric activities. All the datasets were recorded at an interval of 1.0 s. The daily ionospheric activity levels are represented by the average value of the Kp indices (Michel 1964) of that day. Table 3 summarizes the information about the eight datasets.

The characteristics of the eight datasets have very good diversities and representations. First, the levels of ionospheric

Table 3 Description of the eight datasets

Dataset	Collection date	GPS receiver model	Daily average Kp index	GPS station location		
				Station	Latitude (degree)	Longitude (degree)
1	2009-07-22	Ashtech UZ-12	3.1	SHPD Shanghai, China	31.221	121.549
2	2001-04-28	Ashtech UZ-12	4.4	BFTN Bloemfontein, South Africa	−29.104	26.298
3	2009-07-19	Trimble NetRS	0	SHYS Shanghai, China	30.640	122.049
4	2009-07-19	Trimble NetRS	0	SHJS Shanghai, China	30.742	121.344
5	2010-04-10	Trimble NetRS	0.5	BYSP Bayamon Science Park, Puerto Rico	18.408	−66.161
6	2001-03-31	AOA Benchmark	7.6	ALGO Ontario, Canada	45.959	−78.071
7	2004-12-09	Leica SR530	1.875	A buoy in the sea, Hong Kong, China	N/A	N/A
8	2010-01-01	IGOR	0.125	COSMIC Spaceborne C001 L21 (POD2)	N/A	N/A
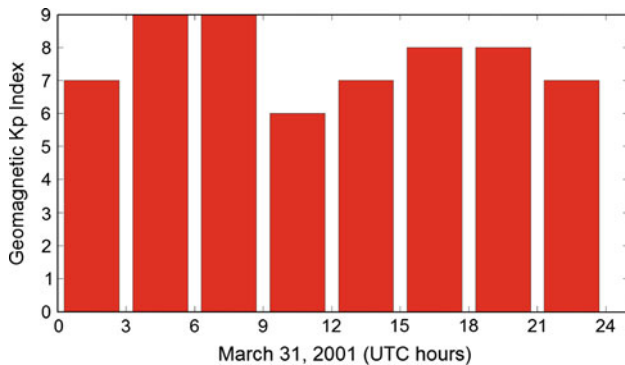
Fig. 1 The geomagnetic Kp index on 31 March 2001

activity varied from very quiet (Kp = 0–0.5) to moderately active (Kp = 3.1–4.4), and to highly active (Kp = 7.6). The eight datasets were collected on different dates and in different years, indicating a good temporal representation. For instance, the dataset 1 was collected by a GPS receiver at Shanghai on 22 July 2009 when a total solar eclipse occurred. The second dataset with high level of ionospheric activities was recorded during the "HIRAC/SolarMax" campaign 23–29 April 2001 (Feltons 2003). The dataset 6 was recorded on 31 March 2001 when a significant geomagnetic storm occurred. The ionospheric TEC were observed to increase to 100 TECU during the 31 March 2001 event (Foster et al. 2002). The average Kp index for that day was 7.6, as shown in Fig. 1. This was the highest daily average Kp index in the past 10 years and the fourth highest in the past 30 years. At the same time, the locations of the GPS receivers had a good geographical distribution over the world. Five different GPS receiver models were tested to see any impact of receiver model on the algorithm's performance. The impact of the GPS receiver dynamics on the performance of the algorithm was also assessed by different datasets: stationary (the first

six datasets), low dynamics (buoyborne receiver in the seventh dataset), and high dynamics (spaceborne receiver in the eighth dataset).

3.2 Test configuration

In this test, three pairs of cycle slip are simulated to evaluate the effectiveness of the method. The simulated cycle slips are added to the GPS data that are then processed by our computer program implementing this algorithm. The first tested simulation cycle slip pair is $(-1, -1)$, which represents -1 cycle on L1 and -1 cycle on L2 carrier phase measurements. The simultaneous occurrence of -1 cycle of slip on both L1 and L2 poses a challenge for many cycle slip detection methods because the using the MWWL ambiguity information cannot detect that. For instance, the detection of $\Delta N_1^p(k) = \Delta N_2^p(k) < 6$ cycles was regarded to be difficult (Blewitt 1990). We simulate the $(-1, -1)$ pair because we want to test the algorithm with the smallest and also the most challenging cycle slip pair $(-1, -1)$. The second and third pairs of simulated cycle slip are $(-77, -60)$ and $(-9, -7)$, respectively. They are chosen because they represent the most and the second most challenging ones to be detected when we use the ionospheric TECR information alone to detect cycle slip. This can be seen in Table 1. When the cycle slip pair is $(-77, -60)$ the artificial TECR caused by the cycle slip is 0.0 TECU/s, and the TECR is -0.030 TECU/s if the cycle slip pair is $(-9, -7)$ with a data rate of 1.0 Hz. The three selected cycle slip pairs represent the most challenging cycle slips to be detected when using either the MWWL ambiguity information alone or the ionospheric TECR information alone. As will be shown in the results, the strength of this algorithm is that with the joint use of MWWL ambiguity and

Fig. 2 The cycle slip simulation start time for each satellite of dataset 1 at SHPD station
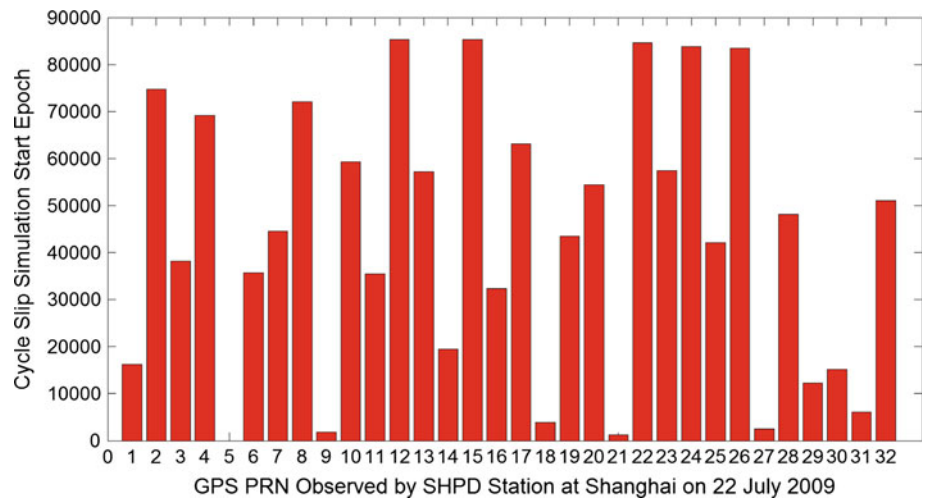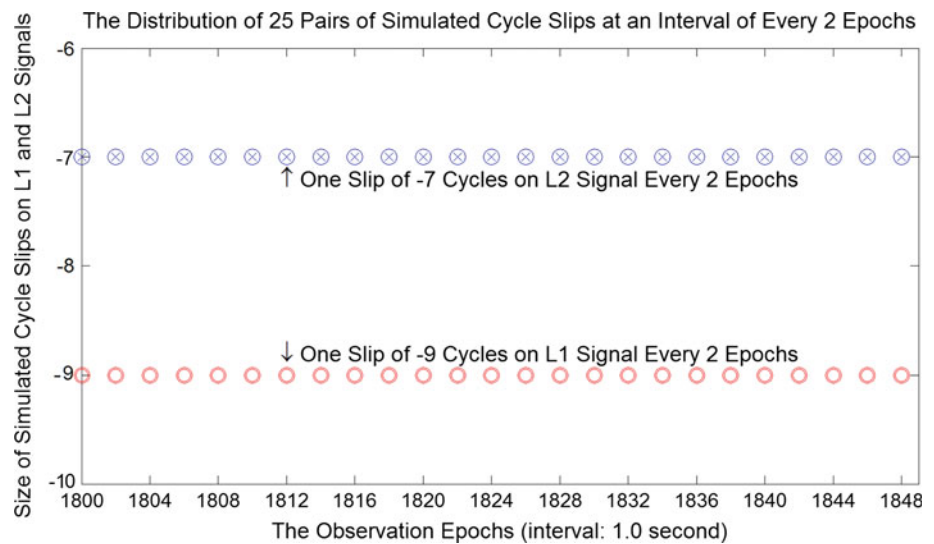

Fig. 3 The distribution of the simulated cycle slips on L1 and L2 signals of PRN 9 of dataset 1

TECR information, virtually any cycle slips can be uniquely detected and repaired.

During a 24-h observation period, one GPS station can usually track approximately 30 satellites. For each satellite in each tested dataset, 25 pairs of cycle slips were simulated. The start time of cycle slip simulation for each satellite was selected randomly. For instance, Fig. 2 showed that the start time of cycle slip simulation for all the satellites tracked at SHPD station in dataset 1. For each satellite, the 25 pairs of cycle slips were consecutively added to its L1 and L2 carrier phase measurements at a two-epoch interval, as shown in Fig. 3. During the 50-epoch period, 25 simulated cycle slips were manually added to the GPS data for cycle slip detection and repair test. The start time of cycle slip simulations for other seven datasets was not shown here, but their start time was essentially random as did the dataset 1.

In Fig. 2, the start time of cycle slip simulation was different for each satellite. However, it is worth pointing out that the start time for each satellite is not required to be different.

This is because this algorithm detects and repairs cycle slips on a satellite-by-satellite basis, and the cycle slip detection for one satellite is not affected by the cycle slips of other satellites. This is confirmed by the test results shown in the following Sect. 3.4.

3.3 Results of using eight GPS datasets

After the simulated cycle slips had been manually added to the L1 and L2 carrier phase measurements, the developed program was executed to detect and repair cycle slips. For all the tested datasets, the number of simulated cycle slips and number of correctly detected and repaired cycle slips were summarized in Table 4. It clearly illustrated that this new algorithm is very effective, and all the cycle slips were successfully detected and repaired except four incorrectly repaired cycle slips in dataset 6. We examined the output data from the program and found that the four incorrectly detected cycle slips in three cycle slip pairs were associated

Table 4 Result of cycle slip detection and repair

Dataset	No. of tracked satellites	Cycle slip pair $(-1, -1)$		Cycle slip pair $(-9, -7)$		Cycle slip pair $(-77, -60)$	
		No. of simulated cycle slips	No. of correctly detected and repaired cycle slips	No. of simulated cycle slips	No. of correctly detected and repaired cycle slips	No. of simulated cycle slips	No. of correctly detected and repaired cycle slips
1	29	775	775	775	775	775	775
2	28	700	700	700	700	700	700
3	29	725	725	725	725	725	725
4	29	725	725	725	725	725	725
5	29	725	725	725	725	725	725
6	29	725	721	725	721	725	721
7	13	325	325	325	325	325	325
8	32	800	800	800	800	800	800

with PRN 7. Further inspection revealed that the pseudorange measurements at GPS Time 20:42:23 had big errors, and they resulted in a sudden increase of the MWWL ambiguity at that epoch. Compared to the MWWL ambiguity calculated one epoch prior to and one epoch after that epoch, the size of the sudden increase is about ten cycles, equivalent to 8.6 m in distance. Thus, the detected cycle slips at that epoch (GPS time 20:42:23) was incorrect. We did not split the data into different arcs when there was a cycle slip; thus, the cycle slip at the epoch 20:42:23 affected the cycle slip detection in the subsequent three epochs. Despite a few incorrect cycle slip detections, the results in Table 4 clearly showed that even if the ionospheric activity was very strong (e.g. dataset 6), the new algorithm could still detect and repair the cycle slips with a very high level of success.

3.4 Comparison with algorithms in online PPP service

The proposed algorithm requires GPS data from one station only, so it is very suitable for the data processing in PPP method. In order to assess the performance of the new algorithm in PPP method, we tested the cycle slip pair $(-77, -60)$ with dataset 5 using the online PPP services provided by two agencies. One is the Global GPS Processing Service (CSRS-PPP) provided by Natural Resources Canada (Héroux et al. 2006), and the other is the Automatic Precise Positioning Service (APPS) provided by Jet Propulsion Laboratory (Bertiger et al. 1998). The online PPP services provide output files containing epoch-by-epoch PPP solutions, which allow us to examine the PPP solutions at all the epochs.

In the dataset 5 from epoch 65500 (GPS Time 18:11:40) to epoch 65548 (GPS Time 18:12:28), a total number of ten GPS satellites were observed at BYSP station, Bayamon Science Park, Puerto Rico. As discussed before, we simulated 25 pairs of cycle slip $(-77, -60)$ on the L1 and L2 signals of the

ten satellites at an interval of every two epochs. The distribution of the simulated cycle slips was illustrated in the Fig. 4.

The fifth dataset with simulated cycle slips were submitted to the online PPP services of NRCan and JPL and processed in static mode. It was unfortunate to find that from time 18:11:40 to 18:12:29, the NRCan outputs had no PPP solution, and the epoch-by-epoch solution series had a 50-epoch (50-s) gap. When the same dataset with simulated cycle slips were uploaded to JPL APPS service, similar problem occurred. From time 18:11:40 to 18:12:28, the APPS outputs had no PPP solution, and the epoch-by-epoch solution series had a 49-epoch (49-s) gap. Compared to NRCan CSRS-PPP service, the JPL APPS had the PPP solution at GPS time 18:12:29. Please note that the last (the 25th) cycle slip simulation was performed at epoch 66548 (GPS Time 18:12:28), as shown in Fig. 4. This can be explained by two possibilities: one is that the online PPP software does not implement cycle slip detection/repair algorithm for the static datasets; the other is that they cannot effectively repair the cycle slips $(-77, -60)$ of all the ten satellites during the 50-s period, so the PPP solution has a gap.

If the GPS data with simulated cycle slips were pre-processed by our algorithm before they were uploaded to NRCan CSRS-PPP service and JPL APPS service, the PPP outputs from both service agencies had no gap during the 50-s (GPS time 18:11:40 to 18:12:29) period. It clearly showed that our new algorithm could effectively detect and repair all the cycle slip pairs $(-77, -60)$ for all the ten satellites during the 50-s period.

To further verify the performance of this algorithm, we reduced the number of satellites with simulated cycle slips from 10 to 9. This time there was no gap in the PPP solutions during the period from GPS time 18:11:40 to 18:12:29. In the NRCan PPP solution, the output file showed that during 18:11:40 to 18:12:29, each epoch's PPP solution used

Fig. 4 The distribution of the simulated cycle slips on L1 and L2 signals of all ten satellites
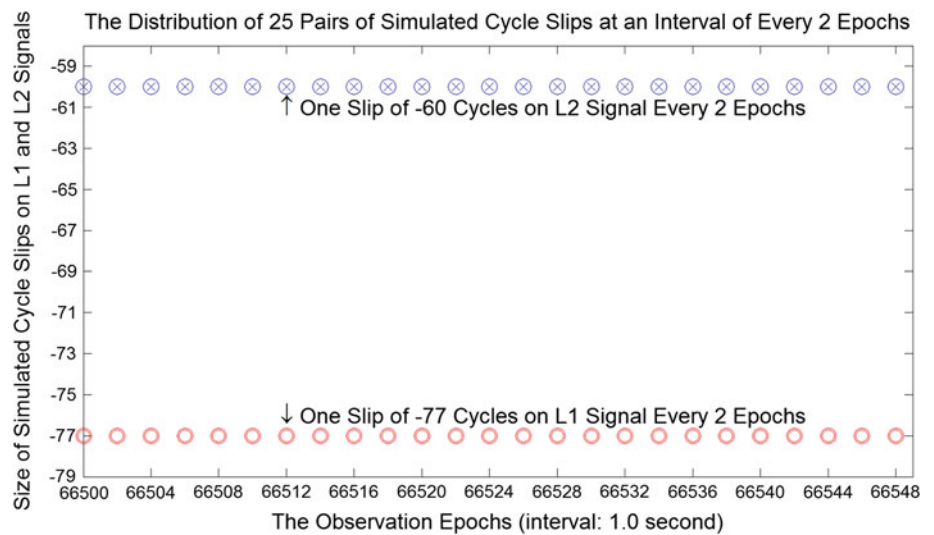
only one satellite. Obviously, the usable satellite is the single satellite that did not have cycle slip simulation. We repeated this for nine times, and each time reduced the number of satellites with cycle slip simulation by one. It was found that each time the number of usable satellites increased by one accordingly. For the JPL PPP solution, there was no information on the number of usable satellites. Therefore, we could not see the change of the number of usable satellites versus the number of satellites with cycle slip simulations.

As said before, the cycle slip pair $(-77, -60)$ is a special cycle slip pair because $[\lambda_1(-77) - \lambda_2(-60)] = 0$. Considering this, we tested another pair of cycle slip $(-20, -3)$ for the same period of GPS time 18:11:40 to 18:12:29 with both NRCan CSRS-PPP and JPL APPS services. Similar results were obtained. When the 25 pairs of cycle slip $(-20, -3)$ were added to all the ten satellites, there was no PPP solution during the 50-epoch period (from 18:11:40 to 18:12:29) in the NRCan CSRS-PPP output file and no solution during the 49-epoch period (from 18:11:40 to 18:12:28) in the JPL APPS output file. We tested another case in the NRCan CSRS-PPP service with only one satellite having $(-20, -3)$ cycle slip simulation, the number of usable satellites increased from 0 from 9. This indicated that the satellite with simulated cycle slip was rejected in CSRS-PPP solution. We were unable to tell how many satellites were rejected since the JPL APPS service did not output the number of usable satellites.

4 Discussion

This new algorithm has been tested extensively using eight datasets with a variety of characteristics. The cycle slips were simulated every second-epoch under low, medium, and high levels of ionospheric activities, which was extremely rare to occur in real-world data collection. It was shown that the algorithm could work effectively to detect very small cycle slips $(-1, -1)$ even under very challenging test situations (with high level of ionospheric activities). The special cycle slip (e.g. $-77, -60$) can also be detected and repaired effectively (the only unrepaired four epochs were caused by abnormality of pseudorange errors).

It should be pointed out this new method succeeds with conditions. First, all the eight datasets used for tests were recorded at a high rate 1.0 Hz. As Table 2 indicates, the same size of cycle slip will result in different TEC rates when the data rate is different. When the data rate is low (e.g. 30 s per GPS observation), the effectiveness of this algorithm is compromised compared to the high data rate cases. For dual-frequency GPS data with low data rate and small size of cycle slips, it will be difficult to detect small cycle slips although the detection of large cycle slips is still possible.

This new algorithm is particularly useful for the precise point positioning technology. The test results showed that this new method may be considered as an option for cycle slip detection and repair in some online PPP services such as NRCan CSRS-PPP and JPL APPS.

5 Conclusion

This paper describes a new method of detecting and repairing cycle slip that is based on the joint use of the ionospheric TECR and MWWL linear combination. In this method, the ionospheric TECR at the epoch of cycle slip detection is compensated by the TECR estimated from previous epochs. The fundamental principle of this new method largely lies in the

fact that the physical (natural) ionospheric TECR is normally considerably smaller than the artificial TECR that is caused by cycle slips. If the calculated TECR exceeds our predefined threshold, it is assumed that cycle slips exist, and the cycle slips on L1 and L2 are determined from the changes of both ionospheric TECR and MWWL ambiguity.

The new algorithm was extensively tested by eight data-sets of different characteristics. A high level of success rate was achieved although a few incorrect cycle slip repairs (but correctly detected) occurred. Our test results showed that in most time the calculated MWWL ambiguities are very accurate. Under very high level of ionospheric activity (the highest in the past 10 years and the fourth highest in the past 30 years), some individual satellites might have a sudden increase of pseudorange errors and degrade the reliability of the MWWL ambiguity, resulting in incorrect cycle slip repair. To further evaluate the performance of our algorithm, we did test with some online PPP services. Our test showed that some online PPP services such as NRCan CSRS-PPP and JPL APPS either have not implemented cycle slip detection and repair algorithms or failed to detect large cycle slips.

This method detects and repairs cycle slip on a satellite-wise basis. The cycle slip detection and repair for each satellite is completely independent and does not rely on the information of other satellites. This explains why even if all the observed satellites at one epoch have cycle slips at the same time, this method can still succeed. Another important feature of this algorithm is that it employs dual-frequency data of only one GPS receiver. This is very suitable for implementation in PPP technique where only one receiver is available. In the differential positioning method, this algorithm can also be used at both reference and rover stations as an extra cycle slip detection and repair method in addition to other methods that use double-differencing data. Naturally, this method can be transformed to process data from other GNSS systems and three-frequency GPS data when three-frequency signals are widely available. To achieve the best performance, the dual- or multi-frequency GPS or GNSS data are recommended to be recorded at 1 Hz or even higher rate.

References

Aoki T, Shimogaki Y, Ikki T, Tanikawara M, Sugimoto S, Kubo Y, Fujimoto K (2009) Cycle slip detection in kinematic GPS with a jerk model for land vehicles. Int J Innov Comput Inf Control 5(1):153–166

Bastos L, Landau H (1988) Fixing cycle slips in dual-frequency kinematic GPS-applications using Kalman filtering. Manuscr Geod 13(4):249–256

Bertiger WI, Bar-Sever YE, Haines BJ, Iijima BA, Lichten SM, Lindqwister UJ, Mannucci AJ, Muellerschoen RJ, Munson TN, Moore AW, Romans LJ, Wilson BD, Wu SC, Yunck TP, Piesinger G, Whitehead ML (1998) A real-time wide area differential GPS system. Navigation. J Navig 44(4):433–447

Bisnath SB, Gao Y (2008) Current state of precise point positioning and future prospects and limitations. In: Proceedings of International Association of Geodesy Symposia: observing our changing earth, vol 133, pp 615–623. Springer, Berlin

Bisnath SB, Langley RB (2000) Automated cycle-slip correction of dual-frequency kinematic GPS data. In: Proceedings of 47th Conference of CASI, Ottawa, Canada

Blewitt G (1990) An automatic editing algorithm for GPS data. Geophys Res Lett 17(3):199–202

Bock H, Dach R, Jäggi A, Beutler G (2009) High-rate GPS clock corrections from CODE: support of 1 Hz applications. J Geod 83: 1083–1094. doi:10.1007/s00190-009-0326-1

Colombo OL, Bhapkar UV, Evans AG (1999) Inertial-aided cycle-slip detection/correction for precise, long-baseline kinematic GPS. In: Proceedings of ION GPS-99, Nashville, TN, pp 1915–1922

Dach R, Schildknecht T, Hugentobler U, Bernier LG, Dudle G (2006) Continuous geodetic time-transfer analysis methods. IEEE Trans Ultrason Ferroelectr Freq Control 53(7):1250–1259

Dai Z, Knedlik S, Loffeld O (2008) Real-time cycle-slip detection and determination for multiple frequency GNSS. In: Proceedings of the 5th workshop on positioning, navigation and communication 2008, Hannover, Germany, pp 37–43

Dai Z, Knedlik S, Loffeld O (2009) Instantaneous triple-frequency GPS cycle-slip detection and repair. Int J Navig Obs 2009:Article ID 407231. doi:10.1155/2009/407231

de Lacy MC, Reguzzoni M, Sans F, Venuti G (2008) The Bayesian detection of discontinuities in a polynomial regression and its application to the cycle-slip problem. J Geod 82: 527–542. doi:10.1007/s00190-007-0203-8

Dow JM, Neilan RE, Rizos C (2009) The International GNSS Service in a changing landscape of Global Navigation Satellite Systems. J Geod 83(3–4):191–198

Fang P, Gendt G, Springer T, Mannucci T (2001) IGS near real-time products and their applications. GPS Solut 4(4):2–8. doi:10.1007/PL00012861

Feltons J (2003) The international GPS service (IGS) ionosphere working group. Adv Space Sci 31(3):635–644

Foster JC, Erickson PJ, Coster AJ, Goldstein J, Rich FJ (2002) Ionospheric signatures of plasmaspheric tails. Geophys Res Lett 29(13):1623. doi:10.1029/2002GL015067

Fotopoulos G, Cannon ME (2001) An overview of multi-reference station methods for cm-level positioning. GPS Solut 4(3):1–10

Gao Y, Li Z (1999) Cycle slip detection and ambiguity resolution algorithms for dual-frequency GPS data processing. Mar Geod 22(4):169–181

Gao Y, Shen X (2002) A new method for carrier phase based precise point positioning. Navigation. J Inst Navig 49(2)

Ge M, Gendt G, Rothacher M, Shi C, Liu J (2008) Resolution of GPS carrier-phase ambiguities in precise point positioning (PPP) with daily observations. J Geod 82:389–399. doi:10.1007/s00190-007-0187-4

Grejner-Brzezinska DA, Kashani I, Wielgosz P, Smith DA, Spencer PSJ, Robertson DS, Mader GL (2007) Efficiency and reliability of ambiguity resolution in network-based real-time kinematic GPS. J Surv Eng 133(2):56–65

Guyennon N, Cerretto G, Tavella P, Lahaye F (2009) Further characterization of the time transfer capabilities of precise point positioning (PPP): the sliding batch procedure. IEEE Trans Ultrason Ferroelectr Freq Control 56(8):1634–1641

Héroux P, Kouba J, Beck N, Lahaye F, Mireault Y, Tétreault P, Collins P, MacLeod K, Caissy M (2006) Space geodetic techniques and the CSRS evolution, status and possibilities. Geomatica 60(2):137–150

Hill EM, Blewitt G (2006) Testing for fault activity at Yucca Mountain, Nevada, using independent GPS results from the BARGEN network. Geophys Res Lett 33:L14302. doi:10.1029/2006GL026140

Hu GR, Khoo HS, Goh PC, Law CL (2003) Development and assessment of GPS virtual reference stations for RTK positioning. J Geod 77(5-6):292–302

Kass WG, Dulaney RL, Griffiths J, Hilla S, Ray J, Rohde J (2009) Global GPS data analysis at the National Geodetic Survey. J Geod 83:289–295. doi:10.1007/s00190-008-0255-4

Kee C, Walter T, Enge P, Parkinson B (1997) Quality Control Algorithms on WAAS Wide Area Reference Stations. J Navig 44(1):53–62

Kim D, Langley RB (2001) Instantaneous real-time cycle-slip correction of dual frequency GPS data. In: Proceedings of the international symposium on kinematic systems in geodesy, geomatics and navigation, pp 255–264

Lee HK, Wang J, Rizos C (2003) Effective cycle slip detection and identification for high precision GPS/INS integrated systems. J Navig 56(3):475–486. doi:10.1017/S0373463303002443

Liu ZZ, Chen W (2009) Study of the ionospheric TEC rate in Hong Kong region and its GPS/GNSS application. In: Proceedings of the international technical meeting on GNSS global navigation satellite system—innovation and application, Beijing, China

Liu ZZ, Gao Y (2004) Development and evaluation of a new 3D ionospheric modeling method. Navigation. J Inst Navig 51(4):311–329

Melbourne WG (1985) The case for ranging in GPS based geodetic systems. In: Proceedings of the 1st international symposium on precise positioning with the global positioning system, Rockville, Maryland, pp 373–386

Michel FC (1964) K_p as a planetary index. J Geophys Res 69(19): 4182–4183. doi:10.1029/JZ069i019p04182

Rizos C (2007) Alternatives to current GPS-RTK services and some implications for CORS infrastructure and operations. GPS Solut 11(3):151–158

Roberts GW, Meng X, Dodson AH (2002) Using adaptive filtering to detect multipath and cycle slips in GPS/Accelerometer bridge deflection monitoring data. In: FIG XXII International Congress, Washington, DC

Schaer S (1999) Mapping and predicting the earth's ionosphere using the global positioning system. PhD dissertation, University of Berne, Berne

Springer TA, Hugentobler U (2001) IGS ultra rapid products for (near-) real-time applications. Phys Chem Earth A Solid Earth Geod 26(6–8):623–628

Sükeová L, Santos MC, Langley RB, Leandro RF, Nnani O, Nievinski F (2007) GPS L2C signal quality analysis. In: Proceedings of Institute of Navigation 63rd annual meeting, Cambridge, MA, pp 232–241

Vollath U, Landau H, Chen X, Doucet K, Pagels C (2002) Network RTK versus single base RTK: Understanding the error characteristics. In: Proceedings of Institute of Navigation GPS 2002, Portland, OR, pp 2774–2781

Wübbena G (1985) Software developments for geodetic positioning with GPS using TI 4100 code and carrier measurements. In: Proceedings 1st international symposium on precise positioning with the global positioning system, Rockville, Maryland, pp 403–412

Xu G (2007) GPS: theory, algorithms and applications. 2nd edn. Springer, Berlin

Zumberge JF, Heflin MB, Jefferson DC, Watkins MM, Webb FH (1997) Precise point positioning for the efficient and robust analysis of GPS data from large networks. J Geophys Res 102:5005–5017